Crystal structure and thermodynamic stability of the lithium alanates $LiAlH_4$ and Li_3AlH_6

O. M. Løvvik
Department of Physics, University of Oslo, P.O. Box 1048 Blindern, NO-0316 Oslo, Norway

Susanne M. Opalka
United Technologies Research Center, 411 Silver Lane, East Hartford, Connecticut 06108, USA

Hendrik W. Brinks and Bjørn C. Hauback
Institute for Energy Technology, P.O. Box 40 Kjeller, NO-2027 Kjeller, Norway
(Received 15 December 2003; published 30 April 2004)

The crystal structure of $LiAlH_4$ and Li_3AlH_6 was determined by density-functional theory (DFT) projector augmented wave ground-state (0 K) minimizations with the generalized gradient approximation (GGA). These results were in excellent agreement with the crystal structure of the deuteride analogs, $LiAlD_4$ and Li_3AlD_6, determined by neutron powder diffraction at 9 K. The DFT calculations were performed by starting with a number of input structures from different space groups. The cell size and shape were allowed to relax, thus making it possible to break or gain symmetry. This was an effective way of searching through a large number of possible symmetries, avoiding less favorable metastable structures. In some cases nearly degenerate structures resulted from quite different starting points, hence providing a good measure of the accuracy of the method. The cell angles differed by up to 0.17°, while the lattice constants and the atomic parameters differed by less than 3 pm, comparable in magnitude to the inherent uncertainty of the GGA. Finite-temperature thermodynamic properties of the alanates predicted with the aid of lattice phonon vibrational simulations were also found to be in good agreement with experimental data. The enthalpies of formation at 298 K for $LiAlH_4$ and Li_3AlH_6 were predicted to be -113.42 and -310.89 kJ mol^{-1}. Similarly, the two reactions, the decomposition of $LiAlH_4$ to form Li_3AlH_6 and the decomposition of Li_3AlD_6 to form LiH, were predicted to have endothermic reaction enthalpies of 9.79 and 15.72 kJ mol^{-1} at 298 K, respectively. This has never been measured directly, and our results may contradict the commonly held belief that pure $LiAlH_4$ is thermodynamically unstable.

DOI: 10.1103/PhysRevB.69.134117 PACS number(s): 61.18.−j, 61.12.−q, 63.20.−e, 71.20.−b

I. INTRODUCTION

The implementation of hydrogen-powered proton exchange membrane fuel cells (PEMFC) in transportation vehicles, portable devices, and temporary housing is dependent upon the development of tractable technologies for conveying and storing hydrogen fuel. Solid-state hydride hydrogen storage is competitive with compressed hydrogen storage, and has the unique combined advantages of high volumetric densities and low parasitic losses. Considerable research is being conducted to develop hydride compounds that can both store high volumetric and gravimetric hydrogen densities, and reversibly charge/discharge hydrogen under the 80–100 °C and 1 atm absolute pressure PEMFC operation conditions. The current renaissance in hydrogen storage research was sparked by the discovery of catalyzed $NaAlH_4$ compositions that have theoretically 5.6 wt. % accessible hydrogen and are reversible under moderate temperature and pressure conditions.[1]

In the drive to improve retrievable hydrogen gravimetric capacity to even higher levels, the focus has been shifted to the investigation of other moderate temperature alkali and alkaline-earth complex hydride compounds. One such system that merits attention is lithium aluminum hydride ($LiAlH_4$), with theoretically 7.9 wt. % hydrogen accessible below 250 °C.[2] Fully charged $LiAlH_4$ releases hydrogen in two decomposition steps upon heating (a third reaction releases hydrogen from LiH, but occurs at too high temperature to be practical for hydrogen storage applications):

$$LiAlH_4 \rightarrow \tfrac{1}{3}Li_3AlH_6 + \tfrac{2}{3}Al + H_2, \quad (1)$$

$$\tfrac{1}{3}Li_3AlH_6 \rightarrow LiH + \tfrac{1}{3}Al + 1/2H_2. \quad (2)$$

The first and second steps can ideally release 5.3 and 2.6 wt. % H relative to $LiAlH_4$, respectively. During rapid heating, $LiAlH_4$ has been reported to first endothermically melt from 165–175 °C, before decomposing and exothermically recrystallizing to form lithium aluminum hexahydride (Li_3AlH_6) over the range of 175–220 °C.[2] The second decomposition step occurs during an endothermic melt reaction over the range of 220–270 °C to form LiH.[2] A recent *in situ* diffraction study of the same system, however, showed that the decomposition temperatures decreased to 112 °C and 127 °C for the two reactions when the heating rate was very low.[3] It was also shown that even at heating rates up to 5 K/min, no melting occurred.[3] It has further been found that $LiAlH_4$ spontaneously decomposes in the solid state to Li_3AlH_6; the half-life of this decomposition was reported to be $\approx$20 years during storage at room temperature.[2] The content of impurities is, however, crucial, since purer samples have significantly higher stability.[4]

The successful catalysis of sodium aluminum hydrides leading to reversible hydrogenation and enhanced kinetics[1] has prompted a search for catalyzed lithium alanate compositions with kinetically enhanced hydrogen discharge and recharge rates that are sufficient for fueling PEMFC under typical operating conditions. However, recent attempts to achieve reversibility in reaction (1) by adding Ti compounds did not have the intended outcome. Solid-state catalysis of $LiAlH_4$ by ball-mill processing with $TiCl_4$,[5] $TiCl_3 \cdot \frac{1}{3}AlCl_3$,[6] or Al_3Ti_5 (Ref. 5) additives resulted in partial to complete solid-state spontaneous decomposition of $LiAlH_4$ to form Al, LiCl, and Li_3AlH_6. Although the Ti-bearing catalysts were successful in eliminating the first melt transformation and lowering the first and second decomposition reaction temperatures by 50–60 °C and 20–25 °C, respectively,[5,6] they promoted the loss of significant hydrogen capacity. A recent study showed that the loss in hydrogen capacity was smaller and the reduction in decomposition temperature was even more significant when $TiCl_3 \cdot \frac{1}{3}AlCl_3$ was replaced by VCl_3.[7] Only the second decomposition reaction has been reported to be partially reversible in the Ti-catalyzed Li_3AlH_6 at 40 bars.[6] So far, catalysts have not been found to successfully invoke full reversibility in the lithium aluminum hydride system.

To this date, the number of theoretical studies on alanate systems is relatively limited. Density-functional theory (DFT) modeling was recently used to resolve the crystal structure of $NaAlH_4$ (Refs. 8 and 9) and Li_3AlH_6 (Ref. 10) and to determine the stable surfaces of $LiAlH_4$.[11] There has not, to our knowledge, been published any calculations on the crystal structure of $LiAlH_4$ and the thermodynamics of the $LiAlH_4$ and Li_3AlH_6 phases.

We have conducted atomic scale simulations of hydride ionic and electronic structures to investigate the observed differences in lithium and sodium aluminum hydrogen phase behavior and their interactions with Ti-based dopants. Our investigations have been enlightened by the recent complete determinations of the $LiAlD_4$ and Li_3AlD_6 structures with combined synchrotron x-ray and neutron diffraction, which resolved the deuterium sublattices for the first time.[12,13] Since analogous hydride and deuteride phases' ionic and electronic structures are virtually identical at the ground state, we will validate our predicted atomic scale hydride structures with these most recent experimental data on lithium aluminum deuteride phases, including newly disclosed powder neutron-diffraction (PND) results on the crystal structure of Li_3AlD_6 at 9 K. We will then analyze the crystal and electronic structures of these phases to further improve our fundamental understanding of complex hydride compound phase behavior.

In order to understand fully the thermodynamic stability of these compounds, it is crucial to elucidate the temperature dependence of the internal energy, enthalpy of formation, etc. We have for the first time, to our knowledge, calculated the phonon vibrational properties of these materials, revealing detailed insight into the thermodynamics of the lithium alanates. Comparisons with experimental results determined on lithium aluminum hydride phases show good correspondence, giving confidence that such methods may also be used in the studies of similar compounds.

II. DENSITY-FUNCTIONAL CALCULATIONS

We have performed band-structure calculations based on DFT with a plane-wave basis set as implemented in the Vienna Ab initio Simulation Package (VASP), which calculates the Kohn-sham ground state by an iterative band-by-band matrix diagonalization scheme and charge density mixing.[14–16] The calculations employed the generalized gradient approximation (GGA) of Perdew and Wang,[17] and the valence electrons were explicitly represented with projector augmented wave (PAW) potentials.[18] The standard version pseudopotentials with the valence configurations that produced the lowest energy structures, Li $2s^1$, Al $3s^2 3p^1$, and H $1s^1$, were employed in this study. The plane-wave cutoff energy was 780 eV and the Gaussian smearing method energy broadening was 0.3 eV. The *k*-point mesh was created by a Monkhorst-Pack scheme[19] using $6\times6\times6$ and $7\times7\times7$ points for $LiAlH_4$ and Li_3AlH_6, respectively. The overall total-energy convergence error for these parameters was well below 1 meV per atom. The convergence criterion for the electronic self-consistent calculations was 0.01 meV/cell.

We conducted a systematic search for the ground-state crystal structure of both $LiAlH_4$ and Li_3AlH_6, using nine and seven different input structures as starting points for the structural optimization of the two compounds, respectively. The starting structures, all belonging to different space groups and representing all the six crystal systems, were based on already known structures from analogous compounds with similar composition stoichiometries. To allow breaking of symmetry, we have started some of the models with cell parameters or positions slightly off the symmetric structure to prevent the VASP program from enforcing the original, higher symmetry. The structure models are listed in Table I and Table II for $LiAlH_4$ and Li_3AlH_6, respectively.

The ground-state (0 K) geometries were determined by minimizing the Hellman-Feynman forces with the conjugate gradient algorithm, until all of the ionic forces were less than 0.05 eV $Å^{-1}$. In order to span a wide range of energetically accessible crystal structures, cell volume, cell shape, and atomic positions were relaxed simultaneously in a series of calculations made with progressively increasing precision. A final high accuracy calculation to calculate the total energy was performed after completion of the relaxation.

Densities of states and crystal orbital overlap populations have been calculated by using ADF-BAND,[34,35] a DFT program using a linear combination of atomic orbitals as basis sets. The relaxed geometries from the VASP calculations were used as input. More details are presented elsewhere.[11]

Elevated temperature vibrational properties of the most favorable structural analogs were predicted with the Materials Design MedeA Phonon package,[36] which invokes a direct supercell approach for simulating the change in lattice thermal vibrational properties.

III. EXPERIMENT

$LiAlD_4$ (Sigma-Aldrich; >95% chemical purity, >98% isotope purity) was heated at 0.15 $Kmin^{-1}$ in vacuum to

TABLE I. The input and resulting output structures from the structural optimization of $LiAlH_4$. The space groups, group numbers, systems, and reference compounds for the input structures are given in the first five columns. The remaining three columns show the relaxed structures' space groups, densities, and the negative of the (uncorrected VASP output) cohesive energies, E_{coh}, per $LiAlH_4$ formula unit. Also listed is the density of the experimental structure linearly extrapolated to 0 K.

Start structure	Group number	System	Based on	Ref.	End structure	Density (kg/m^3)	E_{coh} ($kJ\,mol^{-1}$)
$P\bar{1}$	2	Triclinic	$NaGdCl_4$	(Ref. 20)	$P\bar{1}$	979.9	−1943.8
$P2_1/m$	11	Monoclinic	$KAlF_4$	(Ref. 21)	$P2_1/m$	1049.4	−1920.9
$P2_1/c$	14	Monoclinic	$LiAlD_4$	(Ref. 12)	$P2_1/c$	920.8	−1954.0
$Pnma$	62	Orthorhombic	$KGaH_4$	(Ref. 22)	$Pnma$	1108.0	−1940.9
$I4_1/a$	88	Tetragonal	$NaAlD_4$	(Ref. 23)	$I4_1/a$	1184.2	−1950.2
$P4/mmm$	123	Tetragonal	$KAlF_4$	(Ref. 24)	$P4/mmm$	994.7	−1868.3
$P6_3mc$	186	Hexagonal	$LiBH_4$	(Ref. 25)	$Cmc2_1$	661.9	−1888.4
$P\bar{6}2m$	189	Hexagonal	$CsAlF_4$	(Ref. 26)	$P\bar{6}2m$	909.5	−1896.9
$F\bar{4}3m$	216	Cubic	$NaClO_4$	(Ref. 27)	$F\bar{4}3m$	827.8	−1834.4
Expt.	14	Monoclinic		(Ref. 12)	$P2_1/c$	926.8	

155 °C. All handling of the sample was done in Ar atmosphere in a glove box to prevent reaction with moisture and O_2. The resulting sample mainly consisted of Li_3AlD_6 and Al, but also contained a residue of 12 wt. % LiD and traces of LiCl.

PND data at 9 K were collected with the PUS instrument at the JEEP II reactor at Kjeller (Norway).[37] Monochromatized neutrons with $l=1.5554$ Å were obtained from a Ge(511) focussing monochromator. The detector unit consists of two banks of seven position-sensitive ^{3}He detectors, each covering 20° in 2θ (binned in steps of 0.05°). Data were collected from 10° to 130° in 2θ. The sample was placed in a cylindrical *V* sample holder with 5 mm diameter. The temperature of 9 K was obtained by means of a Displex cooling system. Due to scattering from the cooling system, some angle regions were removed from the PND data (42.0°–43.0°, 46.0°–46.8°, 77.0°–78.0°, and 115.1°–117.8°).

Rietveld refinements were carried out using the program FULLPROF (version 1.9c).[38] The neutron-scattering lengths were taken from the FULLPROF library. Pseudo-Voigt profile functions were used, and the backgrounds were modeled by interpolation between manually chosen points.

IV. RESULTS

A. The structure of $LiAlD_4$ at low temperature

The structural information and the uncorrected cohesive energies output from DFT full cell minimizations on the $LiAlH_4$ structural candidates are presented in Table I. We first note that of all the structures, only the $P6_3mc$ structure underwent a transformation to another space group during

TABLE II. The input and resulting output structures from the structural optimization of Li_3AlH_6. The space groups, group numbers, systems, and reference compounds for the input structures are given in the first five columns. The remaining three columns show the relaxed structures' space groups, densities, and the negatives of the (uncorrected VASP output) cohesive energies, E_{coh}, per Li_3AlH_6 formula unit. Also listed is the density of the present experimental structure linearly extrapolated to 0 K.

Start structure	Group number	System	Based on	Ref.	End structure	Density (kg/m^3)	E_{coh} ($kJ\,mol^{-1}$)
$P1$	1	Monoclinic	$K_3Fe(CN)_6$ [a]	(Ref. 28)	$P2_1/n$	1077.7	−3156.4
$P\bar{1}$	2	Triclinic	Ti_3NiS_6 [a]	(Ref. 29)	$P\bar{1}$	1014.2	−3166.2
$P2_1/n$	14	Monoclinic	Na_3AlD_6	(Ref. 30)	$P2_1/n$	1090.4	−3148.0
$Pna2_1$	33	Orthorhombic	Li_3AlF_6	(Ref. 31)	$Pna2_1$	1027.3	−3157.0
$Immm$	71	Tetragonal	Na_3AlF_6	(Ref. 32)	$Fm\bar{3}m$	1028.9	−3081.8
$R\bar{3}$	148	Rhombohedral	Ti_3NiS_6	(Ref. 29)	$R\bar{3}$	1018.8	−3168.8
$Fm\bar{3}m$	225	Cubic	K_3MoF_6	(Ref. 33)	$Fm\bar{3}m$	1027.8	−3081.8
Expt.	148	Rhombohedral			$R\bar{3}$	1012.2	

[a]The structures with space-group numbers 1 and 2 have been constructed by deliberately breaking symmetry of the structures belonging to group numbers 14 and 148, respectively.

the relaxation calculation. All the structures belonged to different local minima in the crystal space separated by energy barriers on the potential energy surface.

The most stable structure is $P2_1/c$, in correspondence with experimental data. The difference between the energy of the most stable and the second most stable structure ($I4_1/a$) is only about 40 meV, so the $I4_1/a$ is a candidate for a high-pressure high-density phase. Of all the calculated structures, the $P2_1/c$ structure is the only one with the same coordination numbers of hydrogen around its metal atoms as the experimental structure: four around Al and five around Li. Both the experimental and most of the other structures have tetrahedrally coordinated Al-H complexes, the exceptions are $P2_1/m$ (with fivefold coordination), and the $P4/mmm$ and $P\bar{6}2m$ (with sixfold coordination.) The hexagonal $P\bar{6}2m$ structure is the only structure, other than the $P2_1/c$ structure, that exhibits the same fivefold Li-H coordination as the experimental structure. The other structures have Li-H coordination numbers from 6 to 12. The highest number is found in the cubic structure only, which is also the least stable structure of all the ones investigated. Thus, the relatively large variation in coordination numbers among the input structures provided a similarly large variation in stability. It is assuring that the structure with the same coordination numbers (and accordingly similar interatomic distances) as the experimental structure turned out as the most stable structure.

The detailed experimental structure determination of $LiAlD_4$ by combined neutron and x-ray diffraction at 295 K and by PND at 9 K has previously been reported.[12] The structural parameters of the calculated and experimental structures, compared in Table III, are very similar to one another. The calculated lattice constants are less than 2 pm away from the experimental ones, and the monoclinic angle differs by less than 0.1°. None of the atomic positions differs by more than 3 pm. The zero-point motion is not included in this analysis, and we expect that the calculated cell volume would increase by around 1% if zero-point motion were included. Still our calculated results are very close to the experimental values.

TABLE III. Structural parameters for $LiAlD_4$ obtained from refinement of diffraction data at 300 K and 9 K (from Ref. 12), compared to the most stable structure obtained from density-functional calculations at 0 K. The lattice parameters at 0 K using a linear extrapolation of the experimental data are also included. The space group is in all cases $P2_1/c$.

	300 K	9 K	0 K (Extrap.)	0 K (DFT)
a (pm)	48.254	48.174	48.171	48.37
b (pm)	78.040	78.020	78.019	78.09
c (pm)	78.968	78.214	78.191	78.25
γ (deg)	112.268	112.228	112.227	112.137
Li x	0.5601	0.5703		0.5712
Li y	0.4657	0.4656		0.4659
Li z	0.8236	0.8266		0.8263
Al x	0.1428	0.1386		0.1384
Al y	0.2013	0.2033		0.2011
Al z	0.9311	0.9302		0.9312
D1 x	0.1902	0.1826		0.1775
D1 y	0.0933	0.0958		0.0974
D1 z	0.7710	0.7643		0.7601
D2 x	0.3526	0.3524		0.3567
D2 y	0.3726	0.3713		0.3724
D2 z	0.9769	0.9749		0.9768
D3 x	0.2384	0.2425		0.2372
D3 y	0.0840	0.0806		0.0801
D3 z	0.1141	0.1148		0.1149
D4 x	0.8024	0.7994		0.7926
D4 y	0.2644	0.2649		0.2625
D4 z	0.8689	0.8724		0.8712

B. The structure of Li_3AlD_6 at low temperature

The space groups and the calculated cohesive energies for the DFT relaxed possible Li_3AlD_6 structures are shown in Table II. In two cases, the symmetry increased during the ionic relaxation: the $P1$ input structure ended in the $P2_1/n$ space group and the $Immm$ input structure transformed into $Fm\bar{3}m$. The latter final structure model differs by less than 1 pm in both the lattice constants and the atomic positions compared to the model that started as $Fm\bar{3}m$, clearly showing that we have arrived at the same symmetry from two rather different starting points. The two relaxed structures ending with a $P2_1/n$ space group are, on the other hand, not the same. For example the monoclinic angle γ of the structure originating from $P2_1/n$ is 107.65°, while that resulting from the $P1$ structure is 90.80°. In the third case the symmetry also increased, but not enough to fulfill the accuracy of the space-group determination: The final $P\bar{1}$ structure is only slightly distorted from a $R\bar{3}$ symmetry. The angles differ by up to 0.17° and the lattice constants by at most 1 pm from an true $R\bar{3}$ symmetry. This structure is also close to the calculated structure starting from $R\bar{3}$, the difference between the lattice constants being less than 3 pm. The $R\bar{3}$ structure is the most stable structure in Table II, in perfect agreement with the PND results. The structure that started from $P\bar{1}$ is only 30 meV less stable, again reflecting that these structures are degenerate. The difference between the degenerate structures may be understood from the convergence criterion for the structural relaxation being nonzero.

The coordination number of H around the metal atoms between the different calculated structures can be compared in the same manner as with $LiAlH_4$, by treating the structures starting from $Immm$ and $Fm\bar{3}m$ and from $P\bar{1}$ and $R\bar{3}$, respectively, as the same structures. The H atoms are octahedrally coordinated to Al in all structures, with similar Al-H interatomic distances. The Li-H coordination number is 6 for most of the structures. However, for $P2_1/n$, two-thirds of the Li atoms are surrounded in an eight-H atom dodecahedron. Another exception is $Fm\bar{3}m$ with two-thirds of the Li atoms surrounded by 12 H atoms in a perfect icosahedron. Such high coordination numbers are unphysical for so small atoms, and the cubic structure is the least stable of all our

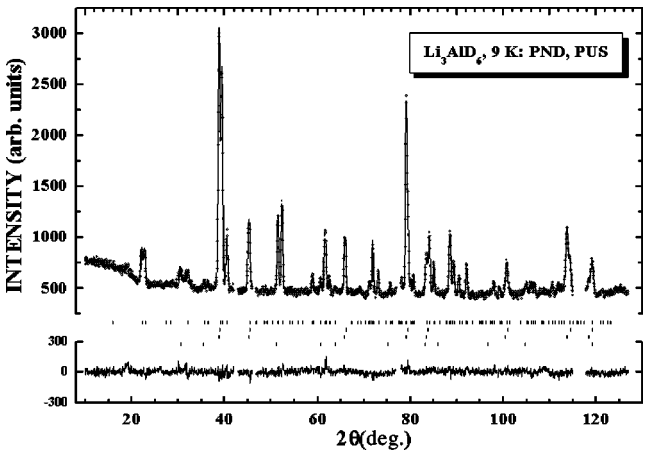

FIG. 1. Observed intensities (circles) and calculated intensities from Rietveld refinements (upper line) of Li_3AlD_6 at 9 K for PND (PUS, Kjeller) data. Positions of Bragg reflections are shown with bars for Li_3AlD_6, Al, and LiD (from top). The difference between observed and calculated intensities are shown with the bottom line.

investigated structures. $P2_1/n$ is also relatively less stable, most probably due to the high H coordination of some of its Li atoms. To explain why the $Pna2_1$ structure is less stable than $R\bar{3}$, we must regard more subtle differences. The two structures have the same coordination number for all atoms, but one Li-H distance is significantly longer in the $Pna2_1$ structure: 25.8 compared to 20.6 pm in the $R\bar{3}$ structure. Another significant difference is that one Li-Al distance is 32.6 pm in the former structure, while all Al-Li distances are shorter than 29 pm in the latter. The $P2_1/n$ derived from the $P1$ has both similar interatomic distances and coordination number as the $R\bar{3}$ structure. The main differences between these structures are the higher degree of distortion and the higher density of the $P1$ structure. Thus, this is a good candidate for a high-pressure phase.

The crystal structure of Li_3AlD_6 at 9 K was determined by Rietveld refinements of PND data. The fit is shown in Fig. 1 and the resulting structural parameters in Table IV. The atomic positions are in good accordance with the room-temperature structure,[13] but the unit-cell dimensions are contracted in the low-temperature results, most significantly along the *c* axis. The thermal expansion coefficient calculated from the experiments is 4.2×10^{-5} K^{-1}. Furthermore, the structural parameters of the experimental and the most stable calculated structure ($R\bar{3}$) are compared in Table IV, revealing very good correspondence between the experimental and calculated structure. The lattice constants differ by less than 2 pm, while the largest difference is found for the Li positions, differing by up to 9 pm. This may be because of the small scattering length of Li, making the PND results for the Li positions less reliable. The cell shape is almost the same; if we look at the structures in rhombohedral setting, the experimental cell has $\alpha=88.56°$, whereas the calculations give $\alpha=88.61°$.

It is interesting to investigate whether the calculated unit cell remains smaller than the experimental unit cell using a slightly different method. We tried to repeat the calculations

TABLE IV. Structural parameters for Li_3AlD_6 obtained from refinement of diffraction data at 300 K (from Ref. 13) and 9 K, compared to the most stable structure obtained from density-functional calculations at 0 K. Unit-cell dimensions extrapolated to 0 K from experimental data are given. The space group is in all cases $R\bar{3}$, and the aluminum positions are (0,0,0) and (0.5,0.5,0.5). Reliability factors for the refinement at 9 K are $R_{wp}=4.30\%$ and $\chi^2=1.08$. The standard deviation is shown in parentheses.

	300 K	9 K	0 K (Extrap.)	0 K (DFT)
a (pm)	48.254	48.174	48.171	48.37
b (pm)	78.040	78.020	78.019	78.09
c (pm)	78.968	78.214	78.191	78.25
γ (deg)	112.268	112.228	112.227	112.137
Li *x*	0.5601	0.5703		0.5712
Li *y*	0.4657	0.4656		0.4659
Li *z*	0.8236	0.8266		0.8263
Al *x*	0.1428	0.1386		0.1384
Al *y*	0.2013	0.2033		0.2011
Al *z*	0.9311	0.9302		0.9312
D1 *x*	0.1902	0.1826		0.1775
D1 *y*	0.0933	0.0958		0.0974
D1 *z*	0.7710	0.7643		0.7601
D2 *x*	0.3526	0.3524		0.3567
D2 *y*	0.3726	0.3713		0.3724
D2 *z*	0.9769	0.9749		0.9768
D3 *x*	0.2384	0.2425		0.2372
D3 *y*	0.0840	0.0806		0.0801
D3 *z*	0.1141	0.1148		0.1149
D4 *x*	0.8024	0.7994		0.7926
D4 *y*	0.2644	0.2649		0.2625
D4 *z*	0.8689	0.8724		0.8712

starting with the $R\bar{3}$ structure, but with the rhombohedral angle fixed at the experimental value, and allowing relaxation of the cell size and atomic positions. This inevitably leads to slightly different lattice constants than our previous method, but the resulting structure from this optimization procedure obtained a cell volume that differs by less than 0.006% from our previously calculated value. The conclusion is that the density of the $R\bar{3}$ structure in Table II is the best available DFT value, where the GGA and the PAW potentials remain as the only important approximations. These approximations give rise to errors in the unit cell size and shape in the same order of magnitude as the error originating from different input geometries.

C. Electronic structure

We have calculated the total and local density of states (DOS) for $LiAlH_4$ and Li_3AlH_6 using the crystal structure from the DFT calculations, and have displayed the occupied valence bands in Fig. 2. The electronic energy levels of the two compounds are predominantly influenced by the mixed tetrahedral (Al-H and Li-Al) and pentagonal (Li-H) coordination in $LiAlH_4$, and the fully octahedral (Al-H, Li-Al, and Li-H) coordination in Li_3AlH_6. The Li_3AlH_6 upper valence

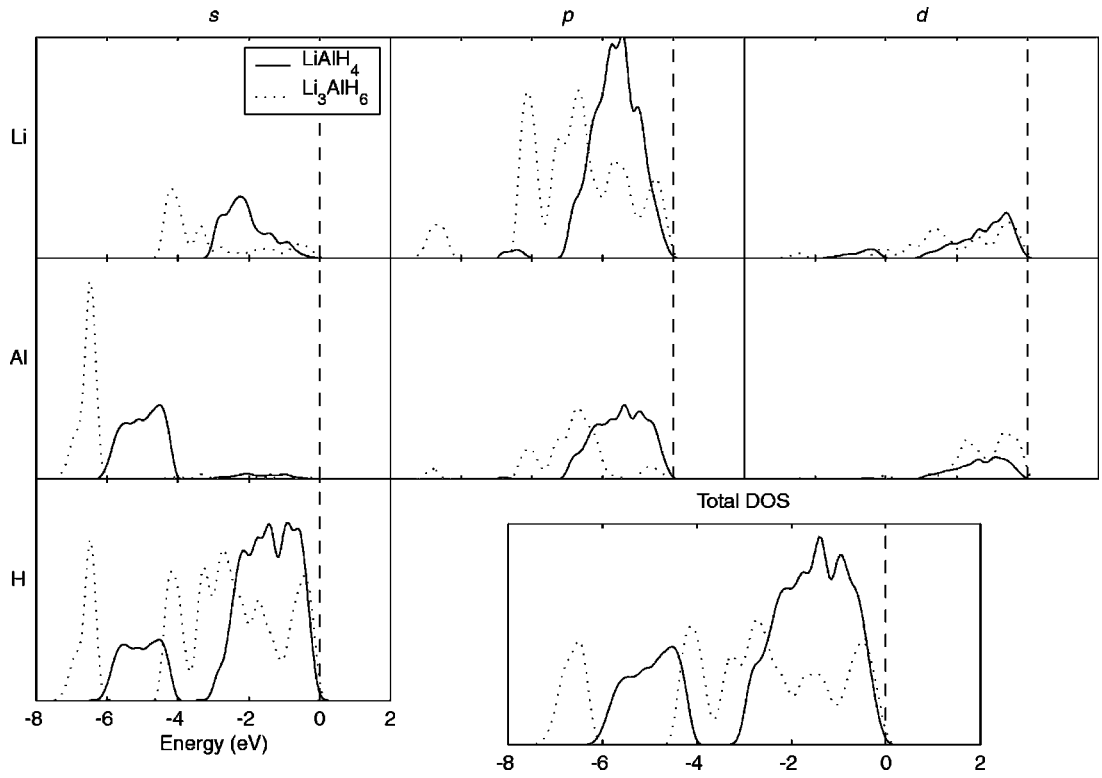

FIG. 2. The calculated local and total density of states (DOS) in arbitrary units for $LiAlH_4$ (solid) and Li_3AlH_6 (dotted). The curves have been smeared out by a Gaussian convolution. The energy is measured in eV relative to the Fermi energy.

band is broader, more complex, and centered further below the Fermi level than for $LiAlH_4$. The Li_3AlH_6 energy levels derived from the hybridization of the lithium $2s$, $2p$, and $2d$ orbitals with the H $1s$ orbitals are distributed throughout, while the hybridization of the Al orbitals with the Li and H orbitals are more localized within the valence band. The Li_3AlH_6 valence band is extended about 2 eV lower in relative energy compared to $LiAlH_4$, by a split-off state originating from the interaction of the H $1s$, Al $3p$, Li $2s$, and Li $2p$ orbitals. The main Li_3AlH_6 valence band is also broader ending about 1 eV below that of $LiAlH_4$.

We have also calculated the crystal orbital overlap population (COOP) for the two lithium alanate phases, shown in Fig. 3. The most important interactions are between the Al and H electrons, being clearly bonding for the *s*, *p*, and *d* electrons of Al. The COOP follows most of the trends as found for the DOS, with more or less the same features seen in both compounds, but with the electrons generally being lower in energy for Li_3AlH_6 than for $LiAlH_4$. A clear difference is, however, the large bonding interaction between Al *s* and H electrons just below the Fermi level for $LiAlH_4$, due to the difference in the crystal-field splitting of the energy levels in the tetrahedral environment. The interaction between Li and H is mainly antibonding, but slightly stronger for $LiAlH_4$ than for Li_3AlH_6. This weaker antibonding interaction between the Li ions and AlH_x complexes may explain the greater stability of the Li_3AlH_6 phase. Certainly, the Li-H interaction does not provide all the details of this interaction, but it serves as a measure of the strength and nature of the interaction.

D. The thermodynamic stability of Li_3AlH_6 and $LiAlH_4$

The relative stability of the various compounds during the phase transformations (1) and (2) is of crucial importance for the practical application of the lithium alanates. We have investigated the thermodynamics of the relevant compounds and reactions by calculating their cohesive energies, formation enthalpies, and reaction enthalpies. The temperature-dependent internal energy E of the various species is the sum of the electronic energy E_{elec} and the molecular kinetic energy consisting of the vibrational energy E_{vib}, the translational energy E_{transl}, and the rotational energy E_{rot}:

$$E(T)=E_{elec}(T)+E_{vib}(T)+E_{transl}(T)+E_{rot}(T). \quad (3)$$

The DFT calculations determine equilibrium structure electronic energies at $T=0$ K, given as an uncorrected cohesive energy determined with respect to non-spin-polarized constituting free atoms. The temperature variation of the electronic energy is generally not significant at low temperatures and was not addressed in this study. The vibrational energy of the solids E_{vib} is given by

$$E_{vib}(T)=E_{vib}(0)+\frac{RT^2}{Q_{vib}}\frac{\partial Q_{vib}}{\partial T}, \quad (4)$$

where the zero-point energy is $E_{vib}(0)=\frac{1}{2}h\Sigma_i n_i$ and Q_{vib} is the partition function for vibrations:[39]

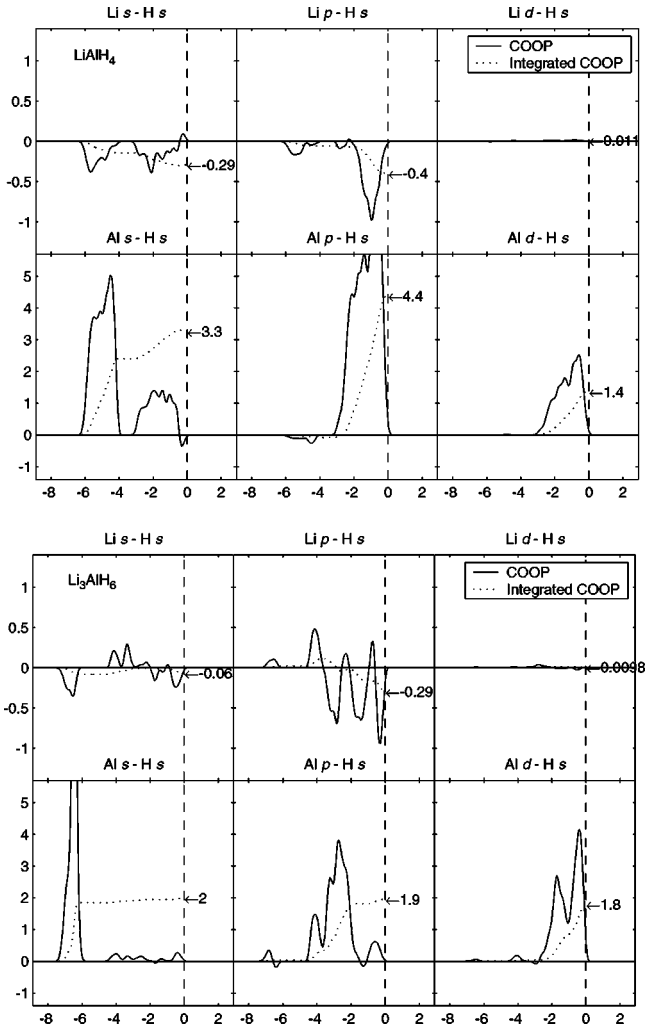

FIG. 3. The calculated crystal orbital overlap population (COOP, full lines) and the integrated COOP (dotted line) for $LiAlH_4$ (top) and Li_3AlH_6 (bottom). The curves have been smeared out by a Gaussian convolution. The energy is measured in eV relative to the Fermi energy.

$$Q_{vib} = \sum_i (1 - e^{-h\nu_i/kT})^{-1}. \quad (5)$$

Lattice phonon vibrational properties were determined by the direct method implemented by Parlinski.[40] In this approach, a dynamic force constant matrix was derived from the Hellmann-Feynman forces resulting from the selective displacement of single atoms from their equilibrium positions in an appropriately constructed supercell. Phonon density of states (DOS) were constructed from the frequency distribution of the normal vibrational modes. The temperature-dependent vibrational contributions to thermodynamic properties were then derived from the integration of the phonon DOS.[40] For the hydrogen molecule, the translational and rotational contributions, as well as the PV contribution, were determined assuming ideal gas behavior.

The enthalpy of formation for $LiAlH_4$ and Li_3AlH_6 with respect to their standard state elemental constituents was calculated at 298 K using the method above, the results are shown in Table I. The predicted formation enthalpies were $H_{form} = -113.42$ for $LiAlH_4$ and $-310.89\ kJ\,mol^{-1}$ for Li_3AlH_6. These predictions were in excellent agreement with the experimentally determined formation enthalpies, ranging from -100.83 to $-122.17\ kJ\,mol^{-1}$,[2,41] and from -298.47 to $-311.0\ kJ\,mol^{-1}$,[2,41] respectively.

Table V also shows the enthalpy of reaction at 298 K H^r_{298} for the reactions (1) and (2). Both are predicted to be endothermic: $H^r_{298} = 9.79\ kJ\,mol^{-1}$ for reaction (1) and $15.72\ kJ\,mol^{-1}$ for reaction (2). The enthalpy of reaction for the decomposition of lithium alanates has to our knowledge never been measured directly before; the only results commonly cited in the literature were reportedly calculated from standard tables of thermal constants.[2] Such calculations give $H^r_{298} = 3.46\ kJ\,mol^{-1}$ for reaction (1) and $14.46\ kJ\,mol^{-1}$ for reaction (2), not too far from our results.[2] It has been claimed that the spontaneous decomposition of $LiAlH_4$ into Li_3AlH_6 in prolonged storage or in long-time ball milling is because of entropy effects, supported by a calculated Gibb's free energy that is negative for the reaction.[2] It has been reported, however, that the level of organic solvent impurities in $LiAlH_4$ is decisive for the spontaneous decomposition; the hydrogen mass density of $LiAlH_4$ is reduced to 32% of the original density after six years' storage when the carbon content is 3 wt. %, it is reduced to 67% after 20 years with 1.86 wt. % carbon, and it is only reduced to 96% after 18 years with 1.04% carbon.[4] Decomposition during high-energy ball milling is only observed after very long milling times (up to 110 h), and is explained by iron contamination introduced during mechanical treatment.[46] It has not been proven that this effect is catalytic only, and that the thermodynamics defies decomposition of the pure $LiAlH_4$. Until this is proven, the possibility is still open that the pure $LiAlH_4$ phase is thermodynamically stable, and that the observed spontaneous decomposition of $LiAlH_4$ to Li_3AlH_6 is due to destabilizing contaminants within the crystal lattice.

V. CONCLUSIONS

The lithium alanates $LiAlH_4$ and Li_3AlH_6 have been studied by state-of-the-art band-structure DFT calculations. The crystal structure of Li_3AlH_6 has also been studied by PND at 9 K. The crystal structure of the alanates was calculated by using a number of structures from different space groups and crystal systems as input. Relaxation of the structures was performed by allowing both the atomic positions, the unit-cell size, and shape to vary, thus making it possible to move away from metastable structures and symmetries. The resulting structures are in excellent agreement with the experimental low-temperature data presented here and elsewhere. The total and local density of states have been calculated, showing that both the Al-H and the Li-H electronic hybridizations are more stable in Li_3AlH_6 than in $LiAlH_4$.

The enthalpy of formation for the alanates at 298 K was also determined by applying vibrational corrections derived from phonon calculations to the cohesive energies obtained from the DFT calculations. These results are in very good correspondence with previous experimental findings. A direct

TABLE V. The heat of formation for $LiAlH_4$ and Li_3AlH_6, and the enthalpy of reaction *Hr* at 298 K for reactions (1) and (2); all in kJ mol^{-1}. The enthalpies of the reactants at 298 K, H^0_{298}, are referenced to their constituent atoms, and were determined by applying the phonon-derived vibrational corrections (and for molecular hydrogen additional translational, rotational, and *PV* corrections) to the uncorrected VASP output cohesive energies.

Reactants H^0_{298} (kJ mol^{-1})							H^r_{298} (kJ mol^{-1})	H^r Expt. (kJ mol^{-1})
Li(s)	+	Al(s)	+	2 H_2(g)	→	$LiAlH_4$(s)		
−150.22		−329.91		−884.92		−1478.47	−113.42	−107.0 (Ref. 2), −107.2 (Ref. 41)
3 Li(s)	+	Al(s)	+	3 H_2(g)	→	Li_3AlH_6(s)		
−450.66		−329.91		−1327.38		−2418.84	−310.89	−298.47 (Ref. 2) [a], −311.0 (Ref. 41)
$LiAlH_4$	→	$\frac{1}{3}$ Li_3AlH_6	+	$\frac{1}{3}$ Al	+	H_2		
−1478.47		−806.28		−219.94		−442.46	9.79	3.462
$\frac{1}{3}$ Li_3AlH_6	→	LiH	+	$\frac{1}{3}$ Al	+	$\frac{1}{2}$ H_2		
−806.28		−459.36		−109.97		−221.23	15.72	14.462

[a]This reaction was not directly reported in Ref. 2. This value was approximated by combining the calculated reaction enthalpies given in Ref. 2, to end up with the desired reaction and associated enthalpy value.

experimental reaction enthalpy measurement for the decomposition of $LiAlH_4$ could not be found in the scientific literature. We report it to be 9.79 kJ mol^{-1}, that is endothermic. The next step in the dehydrogenation, involving the decomposition of Li_3AlH_6, was also predicted to be endothermic with a reaction enthalpy of 15.72 kJ mol^{-1}.

ACKNOWLEDGMENTS

A super computing grant and financial support from the Norwegian Research Council is acknowledged by O.M.L. The generous assistance Paul Saxe of Materials Design is also gratefully acknowledged.

[1] B. Bogdanovic and M. Schwickardi, J. Alloys Compd. **253**, 1 (1997).
[2] T.N. Dymova, D.P. Aleksandrov, V.N. Konoplev, T.A. Silina, and A.S. Sizareva, Russ. J. Coord. Chem. **20**, 263 (1994).
[3] H.W. Brinks, B.C. Hauback, P. Norby, and H. Fjellvåg, J. Alloys Compd. **351**, 222 (2003).
[4] N.N. Mal'tseva and A.I. Golovanova, Zh. Prikl. Khim. (S.-Peterburg) **73**, 705 (2000) [Russ. J. Appl. Chem. **73**, 747 (2000)].
[5] V.P. Balema, J.W. Wiench, K.W. Dennis, M. Pruski, and V.K. Pecharsky, J. Alloys Compd. **329**, 108 (2001).
[6] J. Chen, N. Kuriyama, Q. Xu, H.T. Takeshita, and T. Sakai, J. Phys. Chem. B **105**, 11 214 (2001).
[7] D. Blanchard, H. W. Brinks, B. C. Hauback, and P. Norby, Mater. Sci. Eng. B (to be published).
[8] S.M. Opalka and D.L. Anton, J. Alloys Compd. **356**, 486 (2003).
[9] P. Vajeeston, P. Ravindran, R. Vidya, H. Fjellvag, and A. Kjekshus, Appl. Phys. Lett. **82**, 2257 (2003).
[10] P. Vajeeston, P. Ravindran, A. Kjekshus, and H. Fjellvåg, Phys. Rev. B (to be published).
[11] O.M. Løvvik, J. Alloys Compd. **356-357**, 178 (2003).
[12] B.C. Hauback, H.W. Brinks, and H. Fjellvag, J. Alloys Compd. **346**, 184 (2002).
[13] H.W. Brinks and B.C. Hauback, J. Alloys Compd. **354**, 143 (2003).
[14] G. Kresse and J. Hafner, Phys. Rev. B **47**, 558 (1993).
[15] G. Kresse and J. Furthmuller, Comput. Mater. Sci. **6**, 15 (1996).
[16] G. Kresse and J. Furthmuller, Phys. Rev. B **54**, 11 169 (1996).
[17] J.P. Perdew, J.A. Chevary, S.H. Vosko, K.A. Jackson, M.R. Pederson, D.J. Singh, and C. Fiolhais, Phys. Rev. B **46**, 6671 (1992).
[18] G. Kresse and D. Joubert, Phys. Rev. B **59**, 1758 (1999).
[19] H.J. Monkhorst and J.D. Pack, Phys. Rev. B **13**, 5188 (1976).
[20] T. Schleid and G. Meyer, Z. Anorg. Allg. Chem. **590**, 103 (1990).
[21] J.M. Launay, A. Bulou, A.W. Hewat, A. Gibaud, J.Y. Laval, and J. Nouet, J. Phys. (Paris) **46**, 771 (1985).
[22] S.I. Bakum, A.V. Irodova, S.F. Kuznetsova, O.I. Lyakhovitskaya, Y.Z. Nozik, and V.A. Somenkov, Koord. Khim. **16**, 1210 (1990).
[23] B.C. Hauback, H.W. Brinks, C.M. Jensen, K. Murphy, and A.J. Maeland, J. Alloys Compd. **358**, 142 (2003).
[24] J. Schoonman and R.A. Huggins, J. Solid State Chem. **16**, 413 (1976).
[25] A. Zuttel, S. Rentsch, P. Fischer, P. Wenger, P. Sudan, P. Mauron, and C. Emmenegger, J. Alloys Compd. **356**, 515 (2003).
[26] R. Loesch and C. Hebecker, Z. Naturforsch. B **34**, 131 (1979).
[27] K. Herrmann and W. Ilge, Z. Kristallogr. **75**, 41 (1930).
[28] Y. Morioka, K. Toriumi, T. Ito, A. Saito, and I. Nakagawa, J. Phys. Soc. Jpn. **54**, 2184 (1985).
[29] M. Danot, J. Bichon, and J. Rouxel, Bull. Soc. Chim. Fr. **1972**, 3063 (1972).
[30] E. Rönnebro, D. Noreus, K. Kadir, A. Reiser, and B. Bogdanovic, J. Alloys Compd. **299**, 101 (2000).
[31] J. Burns, A. Tennissen, and G. Brunton, Acta Crystallogr., Sect. B: Struct. Crystallogr. Cryst. Chem. **B24**, 225 (1968).
[32] H.X. Yang, S. Ghose, and D.M. Hatch, Phys. Chem. Miner. **19**, 528 (1993).
[33] L. Toth, G. Brunton, and G. Smith, Inorg. Chem. **8**, 2694 (1969).
[34] G. te Velde and E.J. Baerends, Phys. Rev. B **44**, 7888 (1991).

[35] G. te Velde and E.J. Baerends, J. Comput. Phys. **99**, 84 (1992).
[36] K. Parlinski, *Software Phonon, Cracow*, 2001, as implemented in MEDEA 1.8.
[37] B.C. Hauback, H. Fjellvg, O. Steinsvoll, K. Johansson, O.T. Buset, and J. Jrgensen, J. Neutron Res. **8**, 215 (2000).
[38] J. Rodriguez-Carvajal, Physica B **192**, 55 (1993).
[39] K. K. Irikura, in *ACS Symposium Series*, edited by K.K. Irikura and D.J. Frurip (American Chemical Society, Washington, DC, 1998), Vol. 677, Chap. Appendix B.
[40] K. Parlinski, Z.Q. Li, and Y. Kawazoe, Phys. Rev. Lett. **78**, 4063 (1997).
[41] P. Claudy, B. Bonnetot, J.M. Letoffe, and G. Turck, Thermochim. Acta **27**, 213 (1978).
[42] W.D. Davis, L.S. Mason, and G. Stegeman, J. Am. Chem. Soc. **71**, 2775 (1949).
[43] T. Mukaibo and H. Ryu, Kogyo Kagaku Zasshi **69**, 1693 (1966).
[44] Y.I. Rubtsov, E.P. Kirpichev, and G.B. Manelis, Zh. Fiz. Khim. **43**, 1415 (1969).
[45] K.N. Semenenko, T.S. Il'ina, and V.I. Surov, Zh. Neorg. Khim. **16**, 1516 (1971).
[46] V.P. Balema, V.K. Pecharsky, and K.W. Dennis, J. Alloys Compd. **313**, 69 (2000).